Journal of Advanced Research 43 (2023) 163–174

Contents lists available at ScienceDirect

Journal of Advanced Research

journal homepage: www.elsevier.com/locate/jare

Original Article

CRISPR/Cas9-mediated inactivation of the phosphatase activity of soluble epoxide hydrolase prevents obesity and cardiac ischemic injury

Matthieu Leuillier [a], Thomas Duflot [a,b,c], Séverine Ménoret [d,e,f], Hind Messaoudi [a], Zoubir Djerada [g], Déborah Groussard [a], Raphaël G.P. Denis [h], Laurence Chevalier [i], Ahmed Karoui [j], Baptiste Panthu [k], Pierre-Alain Thiébaut [l], Isabelle Schmitz-Afonso [m], Séverine Nobis [n], Cynthia Campart [n], Tiphaine Henry [n], Camille Sautreuil [o], Serge H. Luquet [h], Olivia Beseme [p], Catherine Féliu [g], Hélène Peyret [g], Lionel Nicol [a], Jean-Paul Henry [a], Sylvanie Renet [a], Paul Mulder [a], Debin Wan [q], Laurent Tesson [d,e,f], Jean-Marie Heslan [d,e,r], Angéline Duché [s], Sébastien Jacques [s], Frédéric Ziegler [t], Valéry Brunel [t], Gilles J.P. Rautureau [u], Christelle Monteil [j], Jean-Luc do Rego [n], Jean-Claude do Rego [n], Carlos Afonso [m], Bruce Hammock [q], Anne-Marie Madec [k], Florence Pinet [s], Vincent Richard [a,b], Ignacio Anegon [d,e,f], Christophe Guignabert [v,w], Christophe Morisseau [q], Jérémy Bellien [a,b,*]

[a] Normandy University, UniRouen, Inserm UMR1096 EnVI, FHU REMOD-VHF, F-76000 Rouen, France
[b] Department of Pharmacology, Rouen University Hospital, F-76000 Rouen, France
[c] Laboratory of Pharmacokinetics, Toxicology and Pharmacogenetics, Rouen University Hospital, F-76000 Rouen, France
[d] Nantes Université, CHU Nantes, Inserm, CNRS, SFR Santé, Inserm UMS 016, CNRS UMS 3556, F-44000 Nantes, France
[e] Nantes Université, CHU Nantes, Inserm, Centre de Recherche en Transplantation et Immunologie, UMR 1064, ITUN, F-44000 Nantes, France
[f] Transgenesis Rat ImmunoPhenomic Platform, F-44000 Nantes, France
[g] Department of Pharmacology, EA 3801, SFR CAP-santé, Reims University Hospital, F-51095 Reims Cedex, France
[h] Unité de Biologie Fonctionnelle et Adaptative, Centre National la Recherche scientifique, Université de Paris, BFA, UMR 8251, CNRS, F-75013 Paris, France
[i] Normandie University, Unirouen, INSA Rouen, CNRS, Groupe de Physique des Matériaux-UMR6634, F-76000 Rouen, France
[j] Normandie Univ, UNIROUEN, UNICAEN, ABTE, F-76000 Rouen, France
[k] CarMeN Laboratory, INSERM, INRA, INSA, Université Claude Bernard Lyon 1, F-69600 Oullins, France
[l] Pathology Department, Rouen University Hospital, F-76000 Rouen, France
[m] Normandie Univ, COBRA, UMR 6014 and FR 3038, Université de Rouen, INSA de Rouen, CNRS, IRCOF, F-76821, Mont-Saint-Aignan, Cedex, France
[n] Animal Behavioral Platform (SCAC), HeRacLeS Inserm US51-CNRS UAR2026, Institute for Research and Innovation in Biomedicine (IRIB), University of Rouen Normandy, F-76183 Rouen, France
[o] Normandie Univ, UNIROUEN, INSERM U1245 and Rouen University Hospital, Department of Neonatal Paediatrics and Intensive Care, F-76000, Normandy Centre for Genomic and Personalized Medicine, Rouen, France
[p] Univ. Lille, CHU Lille, Inserm, Institut Pasteur de Lille, U1167 - RID-AGE - Facteurs de risque et déterminants moléculaires des maladies liées au vieillissement, F-59000 Lille, France
[q] Department of Entomology and Nematology, and UCD Comprehensive Cancer Center, University of California, Davis, CA 95616, USA
[r] GenoCellEdit Platform, F-44000 Nantes, France
[s] Institut Cochin, U1016 INSERM - UMR8104, CNRS - Université Paris Descartes, Genom'IC Platform, Bâtiment Gustave Roussy, F-75014 Paris, France
[t] Department of General Biochemistry, Rouen University Hospital, 76000 Rouen, France
[u] Centre de Résonance Magnétique Nucléaire à Très hauts Champs (FRE 2034, CNRS, Ecole Normale Supérieure de Lyon, Université Claude Bernard Lyon 1), Université de Lyon, F-69100 Villeurbanne, France
[v] INSERM UMR_S 999, Hôpital Marie Lannelongue, F-92350 Le Plessis-Robinson, France
[w] Faculté de Médecine, Université Paris-Sud, Université Paris-Saclay, F-94270 Le Kremlin-Bicêtre, France

Peer review under responsibility of Cairo University.

* Corresponding author at: Department of Pharmacology, Rouen University Hospital, 76031 Rouen cedex, France.
E-mail address: jeremy.bellien@chu-rouen.fr (J. Bellien).

https://doi.org/10.1016/j.jare.2022.03.004
2090-1232/

HIGHLIGHTS

- The physiological role of the phosphatase activity of the bifunctional sEH is unknown.
- CRISPR/Cas9-mediated inhibition of sEH phosphatase in rats induces a lean phenotype.
- Potentiation of brown adipose tissue thermogenesis drives increased energy expenditure in sEH phosphatase knock-in rats.
- sEH phosphatase knock-in rats have an increased cardiac contractility and were protected against cardiac ischemia–reperfusion injury.
- The phosphatase activity of sEH represents a new potential target to fight against obesity and cardiac ischemic complications.

GRAPHICAL ABSTRACT

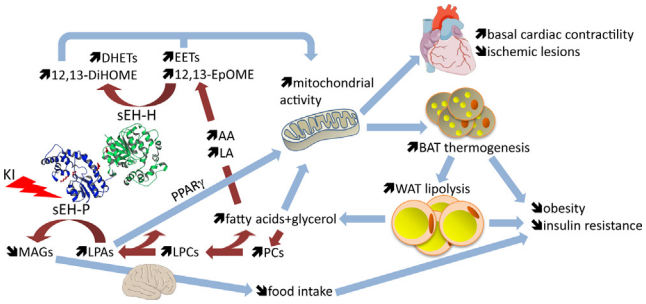

ARTICLE INFO

Article history:
Received 15 December 2021
Revised 28 February 2022
Accepted 2 March 2022
Available online 12 March 2022

Keywords:
Soluble epoxide hydrolase
Lipid phosphatase
CRISPR-Cas9
Thermogenesis
Obesity
Cardiac ischemic injury

ABSTRACT

Introduction: Although the physiological role of the *C*-terminal hydrolase domain of the soluble epoxide hydrolase (sEH-H) is well investigated, the function of its *N*-terminal phosphatase activity (sEH-P) remains unknown.
Objectives: This study aimed to assess *in vivo* the physiological role of sEH-P.
Methods: CRISPR/Cas9 was used to generate a novel knock-in (KI) rat line lacking the sEH-P activity.
Results: The sEH-P KI rats has a decreased metabolism of lysophosphatidic acids to monoacyglycerols. KI rats grew almost normally but with less weight and fat mass gain while insulin sensitivity was increased compared to wild-type rats. This lean phenotype was more marked in males than in female KI rats and mainly due to decreased food consumption and enhanced energy expenditure. In fact, sEH-P KI rats had an increased lipolysis allowing to supply fatty acids as fuel to potentiate brown adipose thermogenesis under resting condition and upon cold exposure. The potentiation of thermogenesis was abolished when blocking PPARγ, a nuclear receptor activated by intracellular lysophosphatidic acids, but also when inhibiting simultaneously sEH-H, showing a functional interaction between the two domains. Furthermore, sEH-P KI rats fed a high-fat diet did not gain as much weight as the wild-type rats, did not have increased fat mass and did not develop insulin resistance or hepatic steatosis. In addition, sEH-P KI rats exhibited enhanced basal cardiac mitochondrial activity associated with an enhanced left ventricular contractility and were protected against cardiac ischemia–reperfusion injury.
Conclusion: Our study reveals that sEH-P is a key player in energy and fat metabolism and contributes together with sEH-H to the regulation of cardiometabolic homeostasis. The development of pharmacological inhibitors of sEH-P appears of crucial importance to evaluate the interest of this promising therapeutic strategy in the management of obesity and cardiac ischemic complications.

Introduction

Almost 30 years after its initial discovery [1,2], it was shown in 2003 that the mammalian soluble epoxide hydrolase (sEH), encoded by the *EPHX2* gene, is a bifunctional protein that not only exhibits a *C*-terminal epoxide hydrolase activity (sEH-H) but also a lipid phosphatase activity on its *N*-terminal domain (sEH-P) (Fig. 1a) [3,4].The sEH-H catabolizes biologically active epoxides generated by cytochrome P450s (CYP450s) from various polyunsaturated fatty acids (PUFAs), including arachidonic acid (AA), linoleic acid (LA), and the omega-3 eicosapentaenoic acid (EPA) and docohexaenoic acid (DHA), to vicinal diols [5–7] (Fig. 1a). In particular sEH-H converts the vasodilator and anti-inflammatory AA-derived epoxyeicosatrienoic acids (EETs) to the less active dihydroxyeicosatrienoic acids (DHETs). A new pharmacological class of inhibitors targeting sEH has been developed and some of them recently reached clinical development to treat cardiometabolic and pain disorders [5–7].

Contrary to sEH-H, little is known about the biological function of sEH-P. Originally thought to only structurally stabilize the sEH-H activity or promote protein dimerization, strong *in vitro* evidence suggests that sEH-P primarily metabolizes intracellular lysophosphatidic acids (LPAs) (Fig. 1a), which are other bioactive phospholipid mediators, to monoacylglycerol (MAGs) [8–11]. In addition, *in vitro* cellular works suggested a complementary role of sEH-H and sEH-P activities in the regulation of metabolic or vascular homeostasis [12–15]. While recombinant mice that do not express ephx2 have been around for some time [16,17], they do not allow to specifically studying sEH-P because both activities are eliminated. However, the differences that have been reported between the effects of sEH genetic knockouts, and those of sEH-H pharmacological inhibition also suggest that sEH-P activity is physiologically relevant [18–20].

While all these findings support the hypothesis for a biological role of sEH-P in particular in the control of cardiometabolic homeostasis, it has yet to be demonstrated. In addition, so far, inhibitors of sEH-P are not fully operational *in vivo* [11]. Therefore, to investigate the biological role of sEH-P in depth, original transgenic rats without sEH-P activity only were generated and their phenotype was studied.

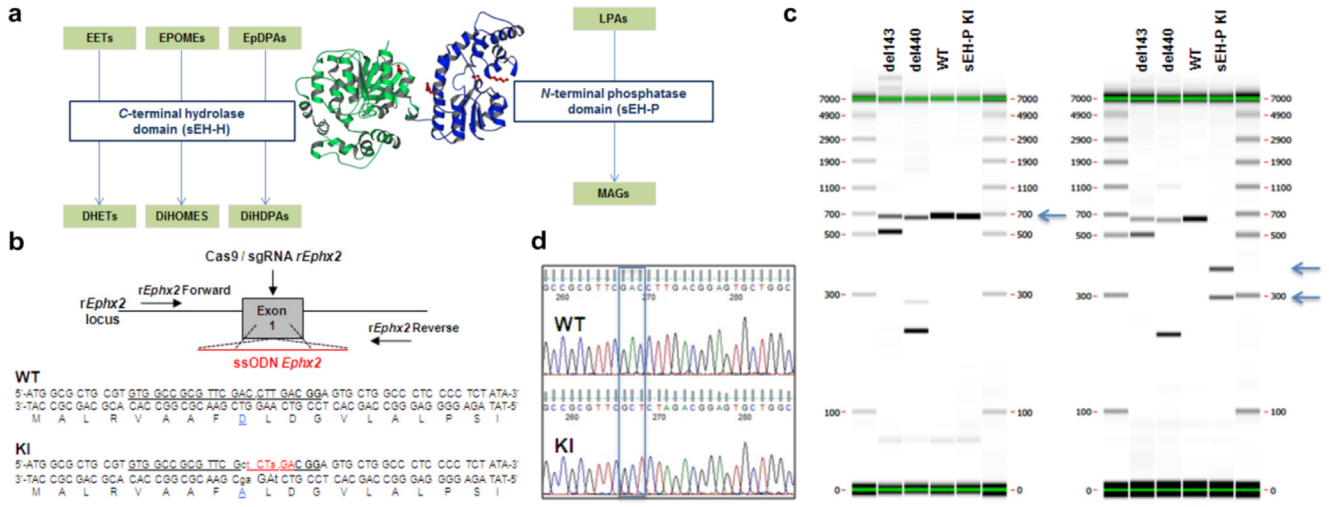

Fig. 1. Generation of sEH-P KI rats. a, Tertiary structure of the sEH protein with the *C*-terminal hydrolase domain (sEH-H) involved in the degradation of epoxyfatty acids *i.e.*, epoxyeicosatrienoic acids (EETs), epoxyoctadecenoic acids (EpOMEs) and epoxydocosapentaenoic acids (EpDPAs) to vicinal diols *i.e.*, dihydroxyeicosatrienoic acids (DHETs), dihydroxyoctadecenoic acids (DiHOMEs) and dihydroxydocosapentaenoic acids (DiHDPAs), and the *N*-terminal phosphatase domain (sEH-P) involved in the degradation of lysophosphatidic acids (LPAs) to monoacylglycerols (MAGs). b, Schematic overview of the rat Ephx2 (rEphx2) gene with WT sequence and sEH-P KI mutation. Exon 1 of rEphx2 was targeted with a single guide RNA (sgRNA, underlined letters in WT sequence with the protospacer-adjacent motif shown in bold), co-delivered with a 100nt single-stranded oligodeoxynucleotide (ssODNs) homologous to the sequence of rEphx2 with modified nucleotides (small letters in KI sequence) to induce a D9A aminoacid substitution (blue aminoacid letters) and introduce a *XbaI* restriction site (red letters) for genotyping and destroying the sequences recognized by the sgRNA. c, left, microcapillary electrophoresis on samples non-digested with *Xba1* from animals del143 and del440 with deletion of respectively 143 and 440 base pairs in one allele and the second allele in WT configuration at ~ 643 bp (blue arrow). KI is evidenced in the right gel (blue arrows) by the two ephx2 PCR fragments after *XbaI* digestion. d, Sanger sequencing analysis of WT and sEH-P KI of rEphx2 with the amino acid substitution allowing the D9A mutation (blue rectangle). (For interpretation of the references to colour in this figure legend, the reader is referred to the web version of this article.)

Materials and methods

Animals and experiments

All experiments involving animals were conducted according to the ethical policies and procedures approved by French Animal Experimentation Ethics Committees (Permit Numbers: Apafis #692, #11484–2017092217377574 and #11920–20171024161 13016).

Detailed methods used for the generation and characterization of sEH-P KI rats are given in the Supplemental materials.

Statistics

The genotype effect was determined by two-tailed unpaired Student's *t*-test or by Mann-Whitney *U* test for non-normally distributed data ($P < 0.05$ on Shapiro-Wilk test) and by one-way repeated measures *ANOVA* with Holm-Sidak *post hoc* test or, for pooled male and female data, by two-way *ANOVA* with gender as the second factor. For the HFD protocols, group effect was determined by one-way *ANOVA* or repeated measures *ANOVA* with Bonferroni's *post hoc* test. Statistical analyses were conducted using GraphPad Prism software 8.0.2. or SPSS Statistics version 8. Data are presented as 1 symbol per rat with mean or mean ± SEM. Two-sided *P* values<0.05 were considered statistically significant.

Results

Generation of sEH-P knock-in (KI) rats

In vivo editing of *EPHX2*: To specifically unravel the role of sEH-P, a targeted gene mutation of *EPHX2* was performed *in vivo* with the substitution of the catalytic nucleophile of sEH-P aspartic acid 9 by alanine (D9A), a mutation known to alleviate totally sEH-P activity *in vitro* [21]. The sEH-P knock-in (KI) Sprague-Dawley rats were generated by using the clustered regularly interspaced short palindromic repeat (CRISPR)-associated (Cas) DNA editing technology as previously described [22,23], with a specific single guide RNA (sgRNA-rEphx2-2.3), Cas9 mRNA and a donor DNA (single-stranded oligodeoxynucleotide; ssODN) (Fig. 1b). The ssODN was designed to generate the D9A mutation, to introduce a restriction XbaI site facilitating the genotyping by PCR and to destroy the sgRNA target sequence to prevent cleavage after KI. KI was detected by microcapillary electrophoresis and further confirmed by Sanger analysis (Fig. 1c-d). Out of 82 pups obtained following embryo microinjection and reimplantation, 17 pups showed indels and 12 pups carried the desired D9A mutation (Supplemental Table 1). Then, founders presenting the D9A mutation were mated with wild-type (WT) rats to derive KI rat lines. Male and female heterozygous rats were intercrossed to obtain the homozygous sEH-P KI and wild-type (WT) rats used for experiments.

Validation of sEH-P KI: In liver tissue, which is characterized by high sEH protein expression [24], the sEH-P activity was nearly undetectable in male and female KI rats compared to WT rats (Table 1). Suppression of sEH phosphatase activity was also demonstrated in interscapular brown adipose tissue (BAT) while, to note, no sEH-P activity was observed in mesenteric white adipose tissue (WAT) even in WT animals from both genders (Table 1). According with the previously suggested role of sEH-P in the conversion of LPAs to MAGs [9–11], LC-MS/MS analysis revealed a decrease in MAG levels and MAG-to-LPA ratios in KI rats but this decrease concerned the most abundant MAG species in plasma *i.e.*, those carrying palmitic or stearic acids (16:0 MAG and 18:0 MAG) in males and those carrying oleic acid or LA in females (18:1 MAG and 18:2 MAG) (Fig. 2a-c and Supplemental Figure 1a). In addition, the plasma levels of most LPAs were slightly increased in male KI rats compared to WT rats but were not modified or unexpectedly reduced in female KI rats (Fig. 2a and Supplemental Figure 1b). However, we detected and demonstrated an increase in 16:0 LPA levels by 45% in male KI rat livers ($P = 0.002$ vs. male WT rats,

Table 1
Microsomal epoxide hydrolase (mEH) activity, soluble epoxide hydrolase (sEH-H) activity and soluble epoxide phosphatase activity (sEH-P) in liver, brown and white adipose tissues (BAT, WAT).

			Specific activity (nmol/min/mg)	
Tissue	**Group**	**sEH-H**	**sEH-P**	**mEH**
Liver	Male WT	3.51 ± 1.11	1.96 ± 0.46	0.26 ± 0.09
	Male KI	5.87 ± 1.28*	0.75 ± 0.37*	0.33 ± 0.14
	Female WT	4.39 ± 0.39	2.32 ± 0.58	0.31 ± 0.07
	Female KI	5.35 ± 0.15*	0.78 ± 0.48*#	0.37 ± 0.10
BAT	Male WT	1.14 ± 0.46	0.16 ± 0.08	0.038 ± 0.006
	Male KI	1.08 ± 0.25	0.003 ± 0.006*#	0.041 ± 0.012
	Female WT	1.51 ± 0.71	0.20 ± 0.11	0.044 ± 0.011
	Female KI	1.28 ± 0.42	0.001 ± 0.002*#	0.040 ± 0.006
WAT	Male WT	0.17 ± 0.09	0.02 ± 0.04#	0.027 ± 0.008
	Male KI	0.14 ± 0.06	0.007 ± 0.007*#	0.024 ± 0.004
	Female WT	0.11 ± 0.07	0.06 ± 0.05#	0.027 ± 0.003
	Female KI	0.10 ± 0.04	0.02 ± 0.02*#	0.029 ± 0.006

Results are mean ± SD (n = 5–9 per group). *P < 0.01 vs. corresponding WT group (Mann-Whitney U test). #P < 0.01: not significantly different from zero. Tissues were obtained from 22-week old male and female sEH-P KI and WT rats.

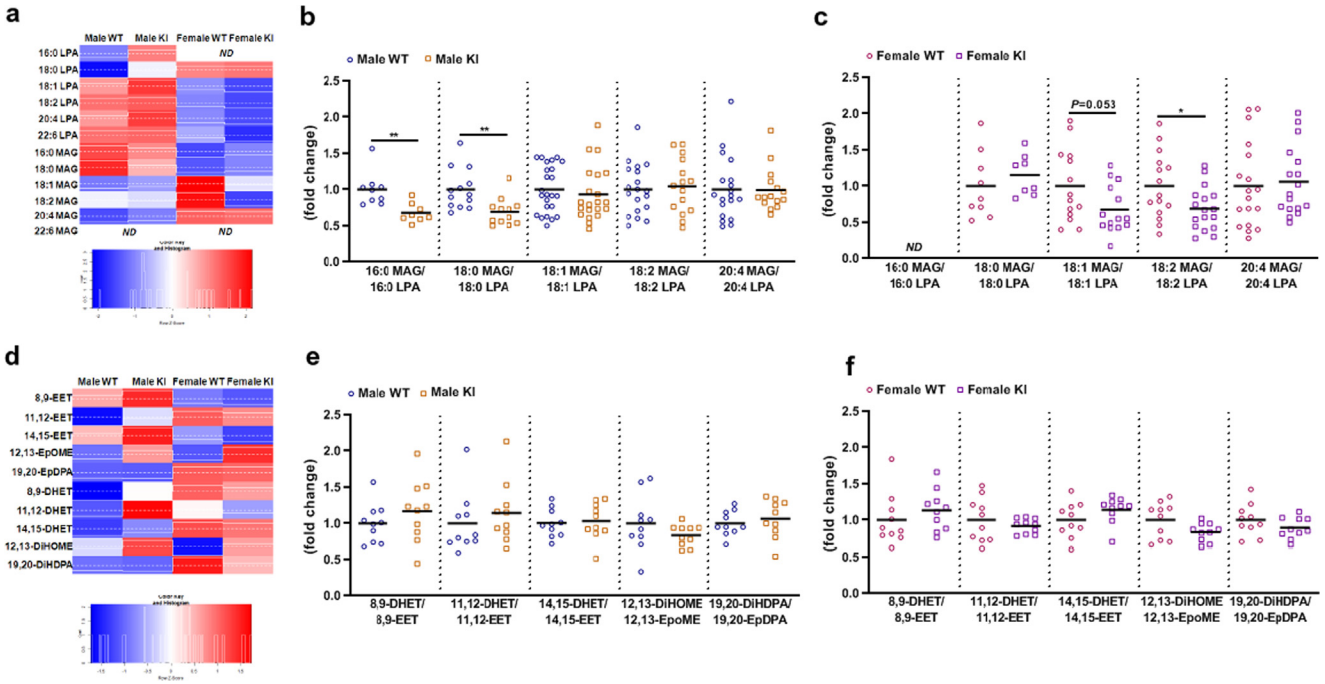

Fig. 2. Impact of sEH-P KI rats on sEH-H and sEH-P substrates and metabolites. a, Heat map shows the differences in the levels of lysophosphatidic acids (LPAs) and monoacylglycerols (MAGs), carrying linoleic (16:0), stearic (18:0), oleic (18:1), linoleic (18:2), arachidonic (20:4) or docosahexaenoic (22:6) acids, quantified in the plasma of 22-week old male and female sEH-P KI and WT rats. Mean values of the male WT group have been used as reference values (see Supplemental Figure 1a-b for numerical values). ND: not detected. b, c, Fold change in LPA-to-MAG ratio quantified in the plasma of 22-week old male (b) and female (c) sEH-P KI and WT rats. d, Heat map shows the differences in the levels of epoxyeicosatrienoic acid (EET) regioisomers, 12,13-epoxyoctadecenoic acid (12,13-EpOME), 19,20-epoxydocosapentaenoic acid (19,20-EpDPA), dihydroxyeicosatrienoic acid (DHET) regioisomers, 12,13-dihydroxyoctadecenoic acid (12,13-DiHOME) and 19,20-dihydroxydocosapentaenoic acid (19,20-DiHDPA) quantified in the plasma of 22-week old male and female sEH-P KI and WT rats. Mean values of the male WT group have been used as reference values (see Supplemental Figure 1c-d for numerical values). e, f, Fold change in EET-to-DHET, 19,20-DiHDPA-to-19,20-EpDPA and 12,13-DiHOME-to-12,13-EpOME ratios quantified in the plasma of 22-week old male (e) and female (f) sEH-P KI and WT rats. b, c, e, f, Mean values are shown. P values represent the genotype effect determined by two-tailed unpaired Student's t-test or by Mann-Whitney U test for non-normally distributed data (P < 0.05 on Shapiro-Wilk test). *P < 0.05, **P < 0.01.

n = 9/ genotype) and by 23% in female KI rat livers (P = 0.031 vs. female WT rats, n = 9/genotype).

On the other hand, sEH-H activity remained detectable in all KI rats and even slightly increased in the liver but not in the BAT or WAT (Table 1). In addition, the KI did not affect the activity of microsomal epoxide hydrolase (mEH) encoded by the *EPHX1* gene (Table 1). As expected, the ratios of DHET regioisomers to EET regioisomers, which can be used as surrogate markers of sEH-H activity, were not modified but a parallel increase in EETs and DHETs was observed in male KI rats (Fig. 2d-f and Supplemental Figure 1c-d). In addition, the ratios of diols to epoxides derived from LA and DHA *i.e.*, 12,13-dihydroxyoctadecenoic acid (12,13-DiHOME) to 12,13-epoxyoctadecenoic acid (12,13-EpOME) and 1 9,20-dihydroxydocosapentaenoic acid (19,20-DiHDPA) to 19,20-epoxydocosapentaenoic acid (19,20-EpDPA) respectively, were not modified (Fig. 2d-f). However, a parallel increase in LA-derived 12,13-EpOME and 12,13-DiHOME was found in both male and female KI rats (Fig. 2d and Supplemental Figure 1c-d), suggesting some form of physiological interaction between both activities of sEH.

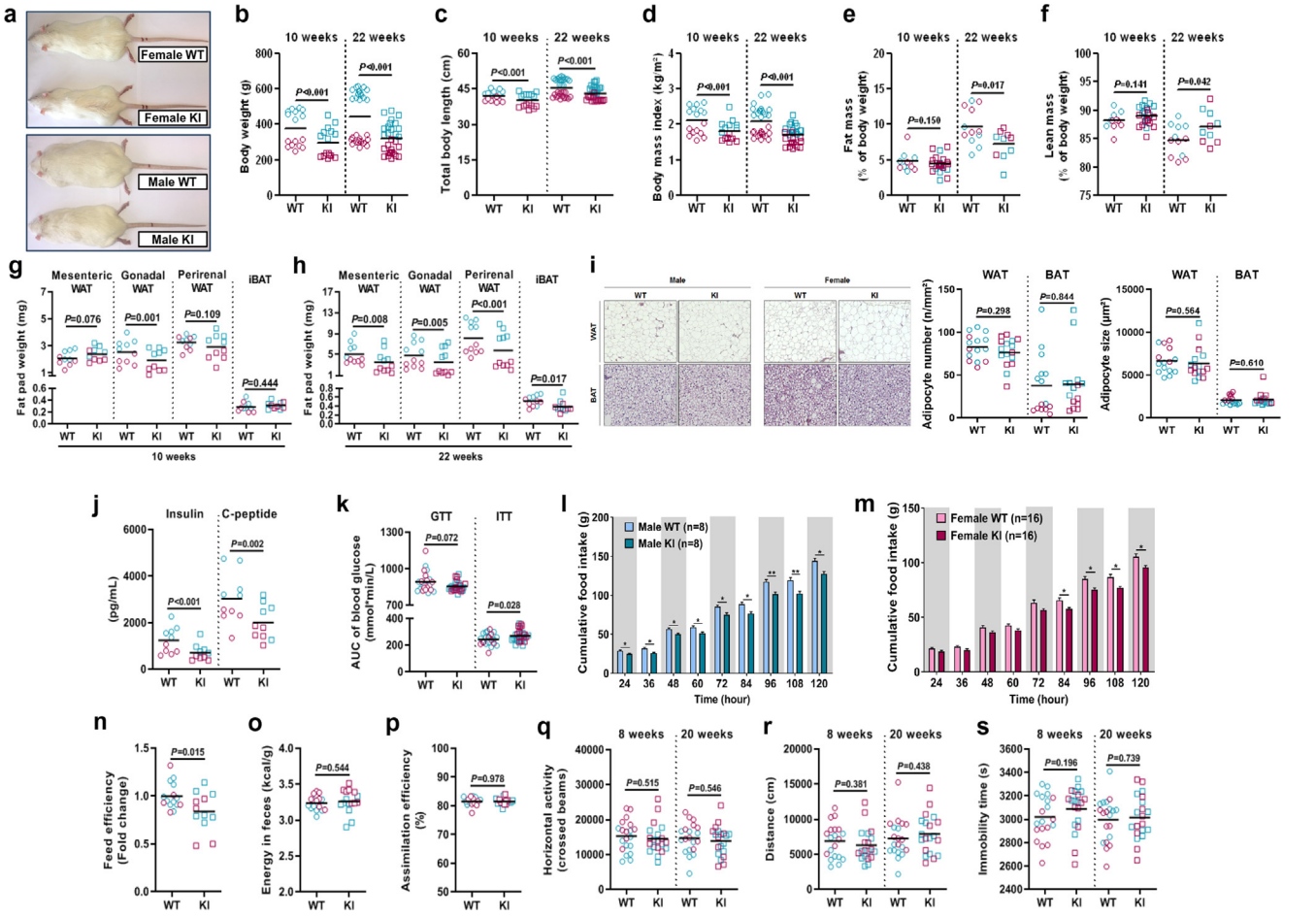

Fig. 3. sEH-P KI promotes a lean phenotype. a-f, Representative photographs (a) of body weight (b), total body length (c), body mass index (d), fat (e) and lean (f) mass relative to body weight, assessed in 10 and 22-week old male (blue) and female (red) sEH-P KI and WT rats. g,h, Mesenteric, gonadal and perirenal white adipose tissues (WAT) and interscapular brown adipose tissue (iBAT) weight assessed in 10 (g) and 22-week old (h) male (blue) and female (red) sEH-P KI and WT rats. i, Representative images of mesenteric WAT (magnification x100) and iBAT (magnification x200) obtained using standard HES staining and quantification of adipocyte number and size in 22-week old male and female sEH-P KI and WT rats. j, Fasting plasma levels of insulin and C-peptide quantified in 22-week old male (blue) and female (red) sEH-P KI and WT rats. k, AUC of blood glucose determined during a glucose and insulin tolerance tests (GTT and ITT respectively) performed in 10 to 20-week old male (blue) and female (red) sEH-P KI and WT rats (see Supplemental Figure 2f-i for the evolution of blood glucose levels during GTT and ITT). l, m, Cumulative food intake assessed in dark and light phases over a period of 5 days using an automated monitoring system in 6 to 8-week old male (l) and female (m) sEH-P KI and WT rats. Grey areas indicate dark periods. n, Fold change in feeding efficiency determined from weight gain and caloric intake (see Supplemental Figure 2a-c) over a period of 120 days in 10-week male (blue) and female (red) sEH-P KI and WT rats. o, p, Fecal energy content (o) and assimilation efficiency (p) determined over a period of 5 days using bomb calorimetry in 6 to 8-week old male and female sEH-P KI and WT rats. q-s, Total horizontal activity (q), distance travelled (r) and immobility time (s) measured during a 60-min open-field test in 8 and 20-week old male (blue) and female (red) sEH-P KI and WT rats. b-k, n-s, Mean values are shown. *P* values represent the genotype effect determined by two-way *ANOVA* with gender as the second factor. The effect of sEH-P KI was more marked in male than in female KI rats for body weight (genotype × gender interaction: $P < 0.001$ at 22 weeks of age), total body length ($P = 0.015$ at 10 weeks and $P = 0.014$ at 22 weeks), and body mass index ($P = 0.024$ at 10 weeks and $P < 0.001$ at 22 weeks). l, m, Mean and SEM values are shown. *P* values represent the genotype effect determined by one-way repeated measures *ANOVA* with Holm-Sidak *post hoc* test. $^{*}P < 0.05$, $^{**}P < 0.01$. (For interpretation of the references to colour in this figure legend, the reader is referred to the web version of this article.)

Loss of sEH-P generates a lean phenotype through a PPARγ-mediated increase in brown adipose tissue thermogenesis

A striking physical trait of female and male sEH-P KI rats was that their markedly lower body weight, measured at 10 and 22-week old, compared with WT rats of the same age (Fig. 3a-b). In addition, total body length (Fig. 3c) and naso-anal length were modestly decreased in KI rats, while tibia length was not significantly affected at 22 weeks (Supplemental Figure 2a-b), suggesting a minor growth defect. Thus, the body mass index (Fig. 3d) and the Lee obesity index (Supplemental Figure 2c) were reduced in KI rats. These effects of sEH-P KI were more marked in male rats (Fig. 3b-d). Moreover, whole-body composition analysis revealed that fat mass was not modified in 10-week-old sEH-P KI rats but was reduced in 22-week-old animals, and this was associated with an increased lean mass (Fig. 3e-f). Accordingly, the weight of the mesenteric, perirenal and perigonadic WAT and interscapular BAT was reduced in KI rats, in particular at 22 weeks of age (Fig. 3g-h), without evidence of morphological difference (Fig. 2i). Although plasma glucose levels under fasted and fed conditions were similar between group as was the fructosamine level (Supplemental Figure 2d-e), sEH-P deficient rats had lesser fasting plasma insulin and C-peptide levels (Fig. 3j), a higher insulin sensitivity and a higher ability to clear glucose from the blood circulation compared to WT rats (Fig. 3k and Supplemental Figure 2f-i). Of note, no difference was found between groups for total cholesterol and triglyceride plasma levels but sEH-P KI induced a decrease in liver weight, in particular in male rats, as well as a reduction in circulating ASAT and ALAT levels and in hepatic lipid content (Supplemental Figure 3a-f).

To decipher the mechanisms underlying the lean phenotype in sEH-P KI rats, food intake was followed up using an automated

monitoring system. A decrease in total food intake was noted in sEH-P KI rats (Fig. 3l-m). The plasma level of the anorexigenic hormone leptin was reduced in sEH-P KI rats (Supplemental Figure 4a), probably due to their lower fat mass, and thus cannot contribute to the decreased rat appetite. In contrast, compared to WT rats, we observed more than a two-fold decrease in the conversion of 20:4 LPA to 20:4 MAG, an endocannabinoid known to stimulate appetite [25], in brain tissue of male sEH-P KI rats (1.0 ± 0.4 vs. 0.46 ± 0.19, n = 6/genotype; P = 0.015). Furthermore, when expressed relative to body weight, the food intake was found to be similar in female WT and sEH-P KI rats and was even greater in male sEH-P KI rats compared to male WT rats (Supplemental Figure 4b-c). The reduction in feeding efficiency in sEH-P KI rats was confirmed within both genders fed a standard chow diet over a period of 120 days (Fig. 3n and Supplemental Figure 4d-f). Neither a change in assimilation efficiency, assessed by quantifying fecal energy content (Fig. 3o-p), nor a modification in spontaneous locomotor activity (Fig. 3q-s) appeared to contribute to the decreased feeding efficiency in sEH-P KI rats.

Next, indirect calorimetry experiments were thus performed in male rats, which exhibit the more pronounced phenotype induced by sEH-P KI. KI rats displayed an increased O_2 consumption and CO_2 production (Supplemental Figure 5a-b), leading to an enhanced overall energy expenditure (Fig. 4a) and a lesser positive energy balance (Supplemental Figure 5c-e). Moreover, the estimated basal metabolic rate was higher (Supplemental Figure 5f) and the respiratory exchange ratio was lower in KI rats (Fig. 4b) especially during the inactive light period, showing a shift in whole-body fuel utilization towards increased fat oxidation (Supplemental Figure 5 g). To assess whether an increased non-shivering thermogenesis may contribute to the increased energy expenditure, core body temperature was continuously measured for 48 h using a telemetry-catheter inserted into the aorta under resting condition. Male KI rats displayed an increased body temperature during both the light and dark periods compared to WT rats (Fig. 4c). Moreover, when submitted to a cold challenge, KI rats had a higher ability to produce heat (Fig. 4d), evaluated by temperature-sensitive transmitters implanted underneath the interscapular BAT, associated with a higher increase in estimated fat oxidation compared to WT rats (Fig. 4e), the main fuel used by BAT to produce heat. In accordance with these results, a transcriptomic analysis of BAT showed a major impact of sEH-P KI on gene expression (Supplemental Figure 6a), with especially an increased expression of the genes coding for proteins involved in thermogenesis and other major linked catabolic pathways including oxidative phosphorylation, tricarboxylic acid (TCA) cycle, fatty acid and glucose metabolism (Fig. 4f-g and Supplemental Figure 6a-c, 7a-c). In addition, an increased expression of the final mitochondrial protein involved in heat generation *i.e.*, uncoupling protein-1 (UCP-1) was confirmed in the BAT of male KI rats (Fig. 4h). To note, core body temperature was also increased in female KI rats compared to WT rats but no change was observed for the cold tolerance test (Supplemental Figure 8a-b), suggesting again a less pronounced phenotype induced by sEH-P KI.

As suggested from blood and urine measurements, the thermogenesis activators catecholamines and thyroid hormones appeared to not contribute to the potentiation of thermogenesis in KI rats and even, triiodothyronine was decreased in sEH-P KI rats (Supplemental Figure 9a-b), suggesting a negative feedback loop to prevent excessive thermogenesis. As previously stressed, leptin that positively regulates thermogenesis was also decreased in sEH-P KI rats (Supplemental Figure 4a). To go further, we next focus on the role of peroxisome proliferator-activated receptors gamma (PPARγ) in sEH KI-induced potentiation of thermogenesis since the increase in intracellular LPAs may promote its activation and because they are known to regulate BAT function [26,27]. Strikingly, 2-week administration of the PPARγ antagonist T0070907 using osmotic minipumps (5 mg/kg/day) totally suppressed the ability of sEH-P KI rats to maintain BAT temperature during a cold tolerance test (Fig. 4, I). In addition, the animals receiving T0070907 for 2 weeks gained more weight compared to non-treated KI animals (31 ± 17 vs. 14 ± 12 g, n = 9/group; P = 0.029).

We then assessed whether an increased turnover and bioavailability of fatty acids that fuel the mitochondria and regulate its functions may contribute to potentiate thermogenesis in sEH-P KI rats. First, an enhanced lipolysis was suggested from the increase in glycerol and fatty acid levels in the plasma of male and female KI rats (Supplemental Figure 9c-d). Lipolysis mostly concerned LA and AA, the latter being in particular elevated in male sEH-P KI rats (Supplemental Figure 9e). According with these results, untargeted lipidomic analyses revealed that the levels of circulating phosphatidylcholine and lysophosphatidylcholine acids were increased in male and female sEH-P KI, especially those containing LA and AA (Supplemental Figure 9f-g), as well as previously shown, some of their metabolites, EETs, DHETs, EpOME and DiHOME (Fig. 2d and Supplemental Figure 1c-d). Because 12,13-DiHOME was shown to potentiate BAT thermogenesis [28], additional cold tolerance tests were performed in male KI rats, which were orally treated 2 weeks with the inhibitor of sEH-H 1-trifluor omethoxyphenyl-3-(1-propionylpiperidine-4-yl) urea (TPPU) to block the formation of this diol. TPPU not only abolished the impact of sEH-P deficiency but even markedly reduced the ability of maintaining interscapular BAT temperature during cold exposure in sEH-P KI rats while it had no effect in WT rats (Supplemental Figure 9 h).

Furthermore, although mean glucose levels appeared similar (Supplemental Figure 2d), glucose telemetry monitoring revealed that glucose levels decreased during the inactive period and increased during the active period to a larger extent in KI rats compared to WT rats (Supplemental Figure 10). This suggests an increased turnover of glucose that may also contribute to thermogenesis as a carbon source for synthesis and rapid oxidation of fatty acids [29,30], which is consistent with the increase in the expression of genes involved in glycolysis and neoglucogenesis (Supplemental Figure 7C). Finally, a NMR-based metabolomic profiling approach performed on the serum of fasted rats showed a decrease in both glycine and betaine levels, suggesting an alteration of the 1-carbon metabolism pathway that could explain the slight growth defect in KI rats, but also decreased citrate levels illustrating alterations in TCA, and TCA-linked lipogenesis (Supplemental Table 2). The variation of acetoacetate levels was expected as it is typical of a change in the ketosis state. As those metabolic pathways are primarily located in the mitochondria, these data support the hypothesis that sEH-P KI profoundly affects mitochondrial metabolism, potentiating catabolic processes while reducing anabolic pathways.

sEH-P KI rats are protected against Diet-Induced obesity and insulin resistance

To determine whether sEH-P may represent a relevant target in insulin resistance, male WT and KI rats were fed with a 60%-containing fat diet (high-fat diet, HFD) during 16 weeks. A control group of WT rats fed with a normal fat diet (NFD) served as controls. The body weight gain of sEH-P deficient rats was reduced compared to WT rats fed a HFD but also unexpectedly, compared to WT rats fed a NFD (Fig. 5a-b). This was due to a decrease in food intake but again feeding efficiency was also lower in sEH-P KI rats compared to WT rats fed a HFD (Fig. 5c-d). In addition, despite the high amount of energy provided by lipid intake, sEH-P deficiency fully prevented the increase in fat mass and decrease in lean mass induced by the HFD (Fig. 5e-g). Quantitative

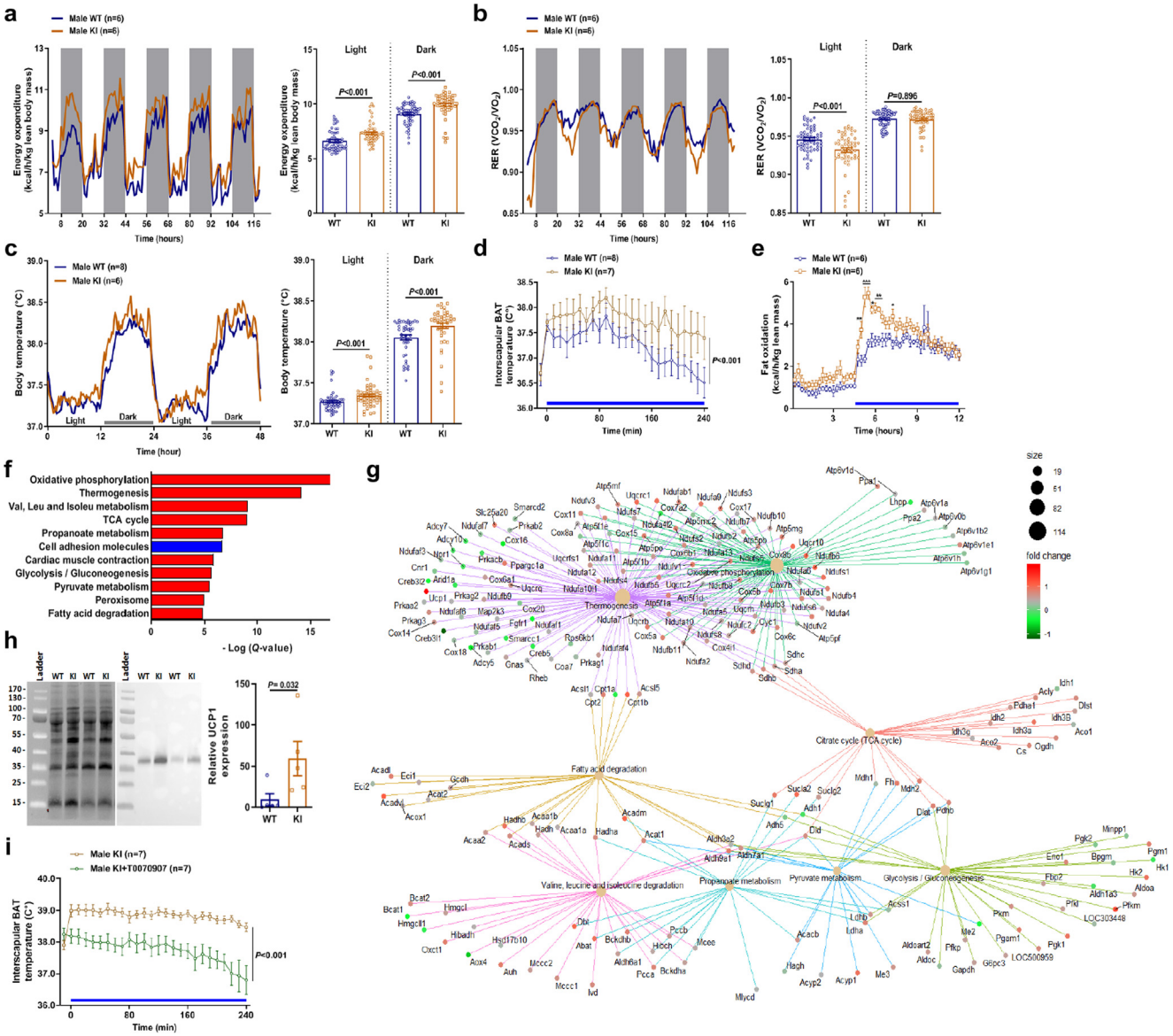

Fig. 4. sEH-P KI increases energy expenditure due to the potentiation of brown adipose tissue thermogenesis. a, b, Absolute and averaged whole-body energy expenditure normalized to lean body mass (a) and respiratory exchange ratio (b) assessed hourly in dark and light phases over a period of 5 days by indirect calorimetry in 12-week old male sEH-P and WT rat. Grey areas indicate dark periods. c, Absolute and averaged core body temperature measured every 15 min in dark and light phases over a period of 48 h using a telemetry-catheter inserted into the aorta of 12-week old male sEH-P KI and WT rats. d, Evolution of interscapular brown adipose tissue (BAT) temperature during a cold tolerance test (6 °C, blue line) performed in 12-week old male sEH-P KI and WT rats. e, Evolution of fat oxidation assessed every 15 min for 12 h by indirect calorimetry before and after switching the room temperature from 24 to 7 °C (blue line) in 12-week old male sEH-P KI and WT rats. f, Barplot of the most significant altered KEGG pathways by sEH-P KI with a Q-value < 0.0001, corresponding to FDR adjustment of the global *P*-value using the Benjamini & Hochberg procedure from *gage* package for R software v3.6.1. Red and blue bars correspond to increased and decreased pathway activity respectively. (g) Gene-concept network depicting the linkage of genes with significantly altered KEGG pathways using *enrichplot* package for R software v3.6.1. Fold changes are log2 transformed (see Supplemental Figure 6a-d for heat maps of gene expressions significantly altered by sEH-P KI). h, Representative stain-free SDS-TGX-gel (left) and Western blot (middle) of uncoupling protein-1 (UCP1) expression quantified (right) in the interscapular BAT of 22-week old male sEH-P and WT rat. i, Evolution of intercaspular BAT temperature during a cold tolerance test (6 °C, blue line) performed in 16-week old male sEH-P KI rats receiving or not the PPARγ antagonist T0070907 during 14 days using osmotic minipumps (5 mg/kg/day). a-c, h, Mean and SEM values are shown. *P* values represent the genotype effect determined by two-tailed unpaired Student's *t*-test or by Mann-Whitney *U* test for non-normally distributed data ($P < 0.05$ on Shapiro-Wilk test). d, i, Mean and SEM values are shown. The *P* value represents the genotype-time interaction effect determined by one-way repeated measures *ANOVA*. e, Mean and SEM values are shown. *P* values represent the genotype effect determined by one-way repeated measures *ANOVA* with Holm-Sidak *post hoc* test. $^{*}P < 0.05$, $^{**}P < 0.01$, $^{***}P < 0.001$. (For interpretation of the references to colour in this figure legend, the reader is referred to the web version of this article.)

fecal fat analysis showed a similar increase in the lipid content of WT and sEH-P KI rats fed a HFD compared to WT fed a NFD, suggesting again no change in lipid absorption (Fig. 5h). Fasting plasma levels of total cholesterol, glucose and fructosamine remained similar between groups but there was a trend for a decreased triglyceride levels in KI rats compared to WT fed a HFD (Supplemental Figure 11a-d). Moreover, sEH-P KI prevented the increase in fasting insulin and C-peptide levels induced by the HFD as well as normalized the insulin tolerance test and liver weight (Fig. 5i-l). A similar protocol of high-fat feeding was then performed to investigate the effects of inhibiting sEH-P in female rats. Although the impact of the HFD was less marked than in male rats, sEH-P deficiency also prevented in female rats the metabolic hallmarks induced by the HFD, including weight and fat mass gain, insulin resistance and hepatic steatosis (Supplemental Figure 12a-j).

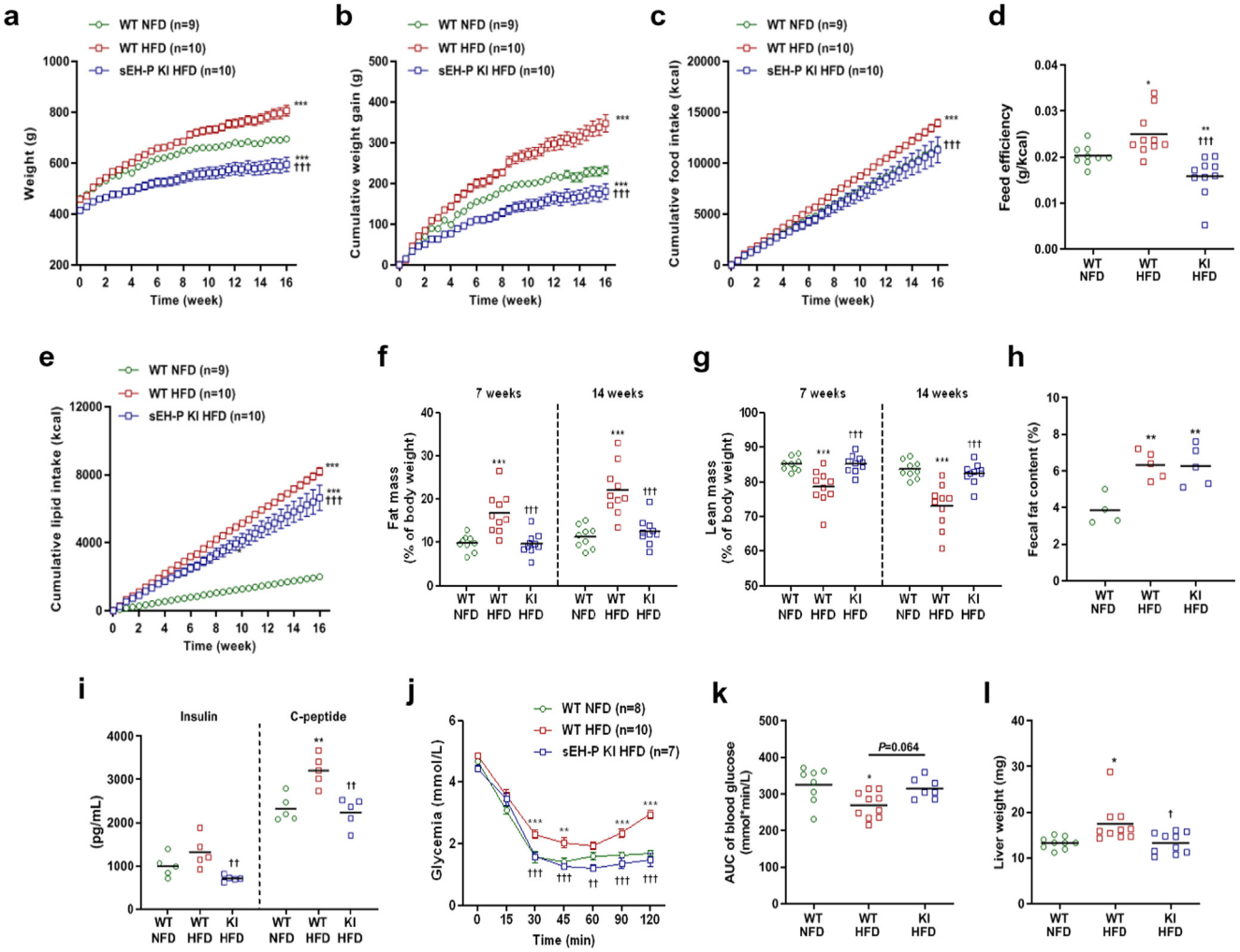

Fig. 5. sEH-P KI male rats are protected against the development of obesity and insulin resistance. a-e, Evolution of body weight (a), cumulative body weight gain (b), cumulative food intake (c), feeding efficiency (d) and cumulative lipid intake (e) assessed in male WT rats fed for 16 weeks a normal food diet (NFD) or a high-fat diet (HFD) and in male sEH-P KI rats fed a HFD. f, g, Fat (f) and lean mass (g) as a percentage of body weight determined 7 and 14 weeks after starting a NFD or a HFD in male WT rats and after starting a HFD in male sEH-P KI rats. h, Lipid fecal content determined over a period of 48 h, 7 weeks after starting a NFD or a HFD in male WT rats and after starting a HFD in male sEH-P KI rats. i-l, Fasting plasma levels of insulin and C-peptide (i), glycemia (j) and AUC (k) of blood glucose determined during an insulin tolerance tests and liver weight (l) assessed 16 weeks after starting a NFD or a HFD in male WT rats and after starting a HFD in male sEH-P KI rats. a-c, e, j, Mean and SEM values are shown and group effect was determined by one-way repeated measures *ANOVA* followed by Bonferroni's *post hoc* test. d, f-i, k, l, Mean values are shown and group effect was determined by one-way *ANOVA* with Bonferroni's *post hoc* test. a-k, $^{*/\dagger}P < 0.05$, $^{**/\dagger\dagger}P < 0.01$, $^{***/\dagger\dagger\dagger}P < 0.001$ compared to NFD and HFD WT rats, respectively.

Loss of sEH-P in rats modifies cardiac mitochondrial architecture and function and protects the heart against Ischemia-Reperfusion injury

Since epoxyfatty acids and sEH play central roles in cardiovascular physiology (5–7), cardiac function and architecture were next examined. Telemetric cardiovascular monitoring showed no change in blood pressure but a trend for an increased heart rate during the active dark period in sEH-P KI rats compared to WT rats (Supplemental Figure 13a-i). Echocardiography showed that left ventricular (LV) posterior and anterior wall thicknesses were not significantly different between groups but LV end-diastolic diameter and mostly LV end-systolic diameter were reduced in male and female KI rats compared to WT, leading to an increase in fractional shortening (Fig. 6a-c). Cardiac MRI confirmed that the reduction in LV volumes was associated with an increase in ejection fraction and actually led to maintain stroke volume (Fig. 6d-f). Similar results were observed at the level of the right ventricle (Supplemental Figure 14a-c). The estimation of myocardial mass by cardiac MRI but mostly the weighting of the different heart cavities showed the decreased cardiac mass in KI rats (Fig. 6g-h and Supplemental Figure 14d). Moreover, the higher cardiac contractility was confirmed by the increase in LV developed pressure in isolated perfused heart from KI rats at baseline but not during beta-adrenergic stimulation with isoproterenol (Fig. 6i).

To address the mechanisms mediating the increased cardiac contractility, transcriptomic and phosphoproteomic analyses were performed on LV tissues from male sEH-P KI and WT rats. In contrast to BAT, the transcriptomic analysis revealed a much less pronounced impact of sEH-P KI at the cardiac level (Supplemental Figure 15). However, there was a lower level of phosphoproteins in LV of sEH-P KI rats compared to WT rats (Supplemental Figure 16a-b). Phosphoproteomic analysis revealed in fact that 4 spots were less phosphorylated in sEH-P KI rats (Fig. 6j-k). Three spots were identified by mass spectrometry and among them 2 mitochondrial proteins of the respiratory chain *i.e.*, ATP synthase subunit beta (ATP5B) and cytochrome *b*-c1 complex subunit 1 (UQRC1) (Fig. 6l). Phos-tag™ gels highlighted differential phospho-species for ATP5B and UQRC1 between WT and sEH-P KI rats, without change in total protein expressions (Fig. 6m-o). Because the impact of the decreased phosphorylation of UQRC1 and ATP5B remains

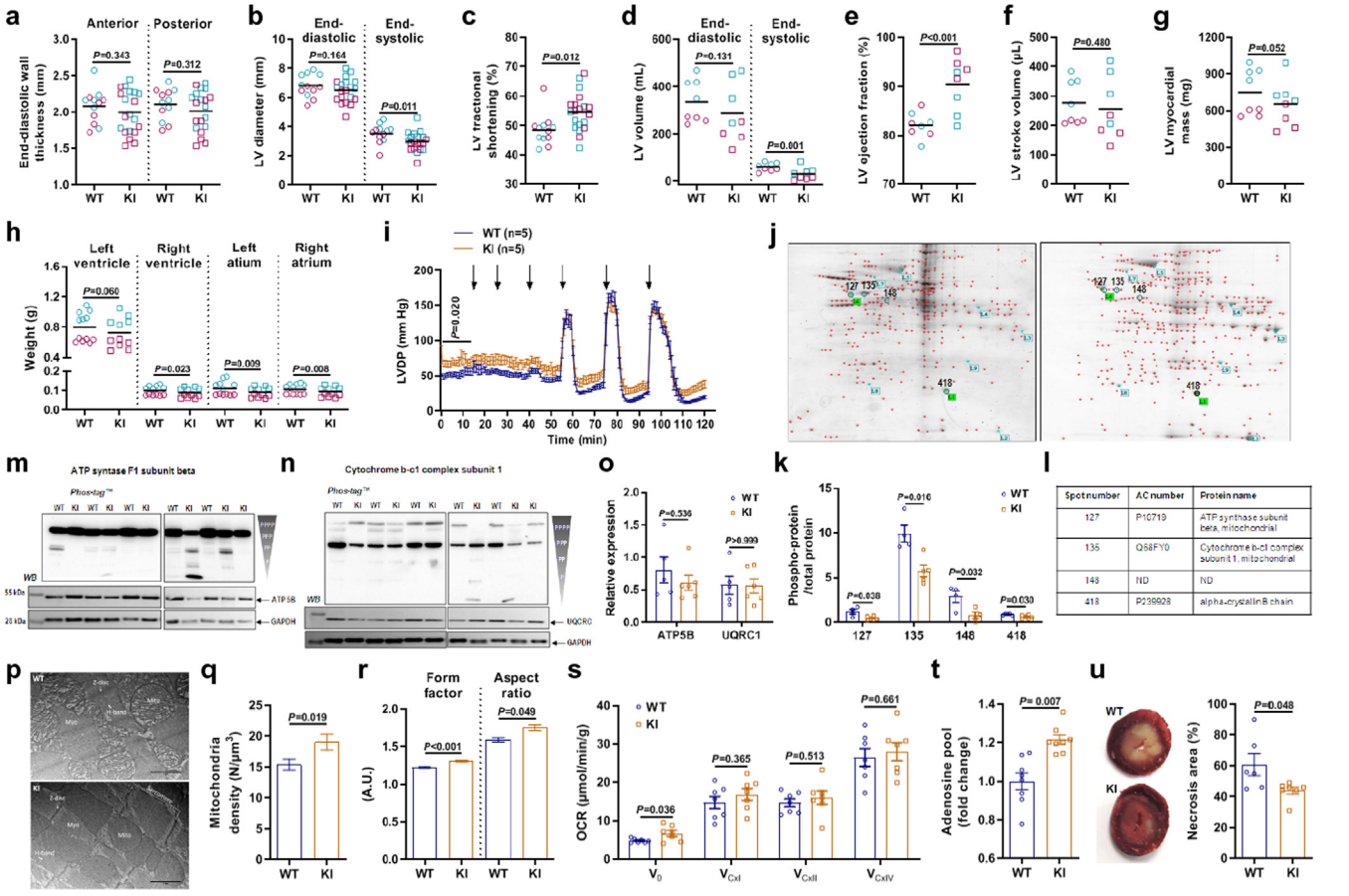

Fig. 6. sEH-P KI increases cardiac contractility and protects the heart against ischemia–reperfusion injury. a-c, Left ventricular (LV) end-diastolic anterior and posterior wall thicknesses (a), LV diastolic and systolic diameters (b) and LV fractional shortening (c) determined by echocardiography in 10-week old male (blue) and female (red) sEH-P KI and WT rats. d-g, LV end-diastolic and end-systolic volumes (d), ejection fraction (e), stroke volume (f) and estimated myocardial mass (g) determined by cardiac MRI in 10-week old male (blue) and female (red) sEH-P KI and WT rats. h, Weight of left and right ventricles and atria assessed in 22-week old male (blue) and female (red) sEH-P KI and WT rats. i, LV developed pressure (LVDP) measured at baseline and during 5-min administration of increasing doses of the beta-adrenergic agonist isoproterenol (from 10^{-11} to 10^{-6} M, black arrows) in perfused hearts isolated from 10-week old male sEH-P KI and WT rats. j, Phosphoproteomic analysis of LV tissues from 10-week old male sEH-P KI (n = 5) and WT (n = 5) rats with an average image of 2D gels established for LV phosphoproteome (left panel) and LV proteome (right panel) using staining by Pro-Q®Diamond and Sypro®Ruby respectively. Phosphorylated polypeptidic spots modulated by sEH-P KI are indicated by a number. k, l, Quantification (k) and identification by mass spectrometry and bioinformatic analysis (l) of spots surrounded with normalized values in 2D gels. ND: not determined. m-o Western blots of phosphorylated ATP synthase subunit beta (ATP5B) and cytochrome *b*-c1 complex subunit 1 (UQRC1) analyzed using Phos-tag™ gels (top panels) and SDS-PAGE gels (bottom panels) with the quantification of total ATP5B and UQRC1 protein expressions normalized to GAPDH expression (o). Each band in Phos-tag™ gels represents a phosphorylated form of the protein, the upper band being the most phosphorylated and the lower band the less or no phosphorylated form of the protein. p-r, Representative micrographs (p) and quantitative analysis of mitochondria numerical density (q), mitochondrial form factor and aspect ratio ® assessed by transmission electronic microscopy in LV tissues obtained from 10-week old male sEH-P KI and WT rats (number of image sections analyzed: n = 46 for KI and n = 51 for WT). Mito: mitochondria; Myo: myofibrils. s, Mitochondrial oxygen respiratory capacity (OCR) assessed by measuring the oxygen consumption rate of skinned LV fibers isolated from 10-week old male sEH-P KI and WT rats in the absence (V_0) or presence of 2 mM ADP with 10 mM glutamate and 4 mM malate (complex I, V_{CxI}), 10 mM succinate and 2 mM amytal, a complex I inhibitor (V_{CxII}), and in the presence of 0.5 mM tetramethyl-p-phenylenediamine (TMPD) and 0.5 mM ascorbate (V_{CxIV}). t, Relative variations of adenosine pool in LV tissues isolated from 22-week old male sEH-P KI and WT rats. u, Representative photomicrographs and quantification of the necrosis area in perfused hearts isolated from 10-week old male sEH-P KI rats and submitted to a 35-min ischemia 60-min reperfusion protocol. a-h, Mean values are shown. *P* values represent the genotype effect determined by two-way *ANOVA* with gender as the second factor. i, Mean and SEM values are shown. *P* value represents the genotype effect determined at baseline before isoproterenol administration by one-way repeated measures *ANOVA*. k, o, q-u, Mean and SEM values are shown. *P* values represent the genotype effect determined by two-tailed unpaired Student's *t*-test or by Mann-Whitney *U* test for non-normally distributed data ($P < 0.05$ on Shapiro-Wilk test). (For interpretation of the references to colour in this figure legend, the reader is referred to the web version of this article.)

elusive [31], additional experiments were performed to explore mitochondrial structure and function. Transmission electronic microscopy analysis revealed discrete LV ultrastructural changes with notably a more regular and parallel arrangement of myofibrils and mitochondria and denser packed cristae in KI rats (Fig. 6p and Extended Table 4). Moreover, quantitative analysis revealed an increase in mitochondria number (Fig. 6q) and in cristae and outer membrane surfaces (Supplemental Figure 17a), as well as mitochondrial remodeling with a more ellipsoidal feature in KI rats, characterized by the increase in Form factor and in aspect ratio (Fig. 6r). This was observed without change in the surface to volume ratio of mitochondria, used as indicator of mitochondrial swelling (Supplemental Figure17b). In accordance with these changes, there was an increased mitochondrial respiration in isolated skinned LV fibers of sEH-P KI rats compared to WT, but this was observed at baseline without difference in stimulated respiratory capacity (Fig. 6s). These results are in accordance with the enhanced basal but not stimulated cardiac contractility and, as already suggested for BAT, support the hypothesis that the increased mitochondrial activity is related to higher substrate availability. Accordingly, the LV adenine nucleotide pool related to ATP production was increased in sEH-P KI rats (Fig. 6t). Further experiments performed on isolated perfused hearts demonstrated that the cardiac necrosis area, representing infarct size, following

ischemia–reperfusion was decreased in sEH-P KI rats (Fig. 6u). This was observed despite a slight reduction in the recovery of cardiac contractility during reperfusion (Supplemental Figure 18-b).

Discussion

In the current study, we provide for the first time definitive evidence that the sEH-P activity plays a physiological role contributing to energy and fat metabolism in the body to regulate cardiometabolic homeostasis.

First, we developed and phenotyped unique genetically-modified sEH-P KI rats to demonstrate that the abolition of sEH-P activity promotes a lean phenotype under physiological conditions and prevents the development of insulin resistance and fat accumulation induced by a HFD. A similar lean phenotype was observed in sEH knockout mice in some studies [32] but not all [16,17], but the respective role of sEH-H and sEH-P activities could not be determined. In the present work, sEH-P KI induced a reduction in food intake that could be related to the decrease in the orexigenic sEH-P metabolite 20:4 MAG in brain [25]. However, the lean phenotype of the KI rats appears mainly related to increased basal energy expenditure notably due to the potentiation of non-shivering thermogenesis in BAT. PPARγ activation was demonstrated to be the triggering event and the associated increase in the bioavailability of fatty acids due to enhanced lipolysis not only fuel the mitochondria but also delivers positive regulators of the heat dissipating machinery. This includes EETs that are also known activators of PPARγ [33] and the cold-induced lipokine 12,13-DiHOME [28]. The demonstration of the suppressing effect of sEH-H inhibition on the potentiation of thermogenesis in sEH-P KI rats supports a role for 12,13-DiHOME but mostly shows that an interaction between the sEH-H and sEH-P activities exists *in vivo*. In fact, previous *in vitro* results suggested that the D9A mutation did not change enzyme structure and sEH-H activity [3,21] and we can hypothesize that the increased sEH-H activity detected at the major site of epoxide hydrolysis, the liver, occur as a functional adaptation to the increase in the availability of its substrates (EETs, EpOMEs), explaining the parallel increase in diols and allowing to maintain a stable epoxide-to-diol ratio. To note, sEH-P appeared to play a minor role in the WAT but BAT activation alone is known to promote WAT fatty acid mobilization and release [34].

Thermogenesis is a fundamental mechanism that helps animals to maintain body temperature in endothermic organisms, *i.e.* in mammals and birds. Interestingly, ectothermic organisms that depend primarily upon external heat sources and behavioral and physiological adjustments to thermoregulate *i.e.*, fish, amphibian and reptile, lack the sEH-P domain, which has been found only in mammals [35]. This suggests that the evolutionary event leading to a bifunctional sEH may be natural selection step contributing to the development of thermogenesis regulation in mammals [36]. Furthermore, it remains to be determined whether the less marked metabolic phenotype of female KI is due to the estrogen-dependent downregulation of sEH expression [37]. This could contribute to the recently demonstrated gender-specific response to cold [38].

Importantly, sEH-P KI also allowed to fully prevent weight gain and all the metabolic abnormalities induced by a HFD and this beneficial impact was observed in both male and female rats. These astonishing results appeared again to rely on the decrease in food intake and efficiency but may also be partly explained by the increase in epoxyfatty acids, in particular EETs. Indeed, EETs were shown to prevent glucose homeostasis abnormalities by preventing insulin resistance and inducing insulin release [39,40]. In this respect, sEH-H inhibition was also shown to improve insulin resistance markers in similar feeding conditions than in the present work [18]. However, compared to sEH-P KI, the improvements with the sEH-H inhibitors appeared only partial and no change in weight gain was usually reported [18,41].

Second, at the cardiac level, a modification in mitochondrial ultrastructure and a similar potentiation of mitochondrial activity seems to drive an increased basal contractility associated with sEH-P KI. Although positive inotropism may worsen energetic imbalance of the myocardium during ischemia and reperfusion situations, sEH-P KI was associated with a preventive effect against ischemia–reperfusion lesions. The reduced post-ischemic recovery of cardiac contractility suggests in fact that sEH-P may improve the matching metabolic capacity of the tissue with cardiac work after ischemia, preventing overstimulation and contributing to the reduction in infarct size [42].

Although we cannot definitely extrapolate our results to human, the role of sEH-P is also suggested by genetic studies showing that the presence of the EPHX2 R287Q polymorphism, known to reduce sEH-H activity but also sEH-P activity toward LPAs [24,43], is associated with higher insulin sensitivity and a reduced risk of developing diabetic nephropathy [44,45]. Moreover, the *EPHX2* K55R polymorphism that increases both activities may precipitate cardiovascular thrombotic events and aggravate patient prognosis [46,47].

Altogether, the results of the present work highlight the pivotal role played by sEH-P in energy and fat metabolism, contributing together with sEH-H to the regulation of cardiometabolic homeostasis. The development of pharmacological inhibitors of sEH-P appears thus of crucial importance to evaluate the interest of this promising therapeutic strategy in the management of obesity and insulin resistance and to prevent cardiac ischemic complications. In fact, improvements in pharmacokinetic properties of recently-developed inhibitors of sEH-P are needed to reduce oral doses and off-target effects, including sEH-H inhibitory activity, before being tested in animal models.

Compliance with ethics requirement

All the animal care and procedures were approved by French Animal Experimentation Ethics Committees and performed in accordance with the guidelines from the French National Research Council for the Care and Use of Laboratory Animals (Permit Numbers: Apafis #692, #11484-2017092217377574 and #11920-2017102416113016).

CRediT authorship contribution statement

Matthieu Leuillier: Validation, Formal analysis, Investigation, Data curation, Writing – review & editing, Visualization. **Thomas Duflot:** Methodology, Validation, Formal analysis, Investigation, Data curation, Writing – review & editing, Visualization. **Séverine Ménoret:** Validation, Investigation. **Hind Messaoudi:** Investigation. **Zoubir Djerada:** Methodology, Investigation, Writing – review & editing. **Déborah Groussard:** Investigation. **Raphaël G. P. Denis:** Methodology, Investigation. **Laurence Chevalier:** Methodology, Investigation. **Ahmed Karoui:** Investigation. **Baptiste Panthu:** Investigation. **Pierre-Alain Thiébaut:** Investigation. **Isabelle Schmitz-Afonso:** Investigation. **Séverine Nobis:** Investigation. **Cynthia Campart:** Investigation. **Tiphaine Henry:** Investigation. **Camille Sautreuil:** Investigation. **Serge H. Luquet:** Investigation. **Olivia Beseme:** Investigation. **Catherine Féliu:** Investigation. **Hélène Peyret:** Investigation. **Lionel Nicol:** Investigation. **Jean-Paul Henry:** Investigation. **Sylvanie Renet:** Investigation. **Paul Mulder:** Investigation. **Debin Wan:** Investigation. **Laurent Tesson:** Investigation. **Jean-Marie Heslan:** Investigation.

Angéline Duché: Investigation. **Sébastien Jacques:** Investigation. **Frédéric Ziegler:** Investigation. **Valéry Brunel:** Investigation. **Gilles J.P. Rautureau:** Investigation. **Christelle Monteil:** Investigation. **Jean-Luc do Rego:** Methodology, Resources, Writing – review & editing. **Jean-Claude do Rego:** Methodology, Resources, Writing – review & editing. **Carlos Afonso:** Methodology, Resources. **Bruce Hammock:** Methodology, Resources, Writing – review & editing, Supervision. **Anne-Marie Madec:** . **Florence Pinet:** Methodology, Resources, Writing – review & editing. **Vincent Richard:** Resources, Supervision. **Ignacio Anegon:** Conceptualization, Methodology, Validation, Resources, Data curation, Writing – review & editing, Supervision. **Christophe Guignabert:** Conceptualization, Methodology, Validation, Resources, Data curation, Writing – review & editing, Supervision. **Christophe Morisseau:** Conceptualization, Methodology, Validation, Formal analysis, Resources, Data curation, Writing – review & editing, Supervision. **Jérémy Bellien:** Conceptualization, Methodology, Validation, Formal analysis, Investigation, Resources, Data curation, Writing – original draft, Writing – review & editing, Visualization, Supervision.

Declaration of Competing Interest

The authors declare that they have no known competing financial interests or personal relationships that could have appeared to influence the work reported in this paper.

Acknowledgments

The authors thank Dr. Sophie Claeyssens for the determination of fecal fat content (Department of General Biochemistry, Rouen University Hospital, France), Dr. Ly Tu and Dr. Raphaël Thuillet for their help in the characterization of sEH-P rats (INSERM UMR_S 999). The authors acknowledge the technical platform metabolism of the Unit "Biologie Fonctionnelle et Adaptative" (Université de Paris, BFA, UMR 8251, CNRS, F-75013 Paris, France) for calorimetric analysis.

This study was supported by grants from the French National Research Agency (ANR-16-CE17-0012), the National Institute of Health (R35 ES030443, R15 DK114790, and P42 ES004699) and European Union and Normandie Regional Council. Europe gets involved in Normandie with European Regional Development Fund (ERDF). M.L. was recipient of Normandy Regional Council fellowship. In addition, the development of the sEH-P KI rats was financially supported by the "TEFOR" project funded by the "Investissements d'Avenir" French Government program, managed by the French National Research Agency (ANRII INSB-0014). This work was supported at COBRA laboratory by the European Regional Development Fund (ERDF, no. HN0001343), Labex SynOrg (ANR-11-LABX-0029) and Région Normandie.

Appendix A. Supplementary material

Supplementary data to this article can be found online at https://doi.org/10.1016/j.jare.2022.03.004.

References

[1] Gill SS, Hammock BD, Casida JE. Mammalian metabolism and environmental degradation of the juvenoid 1-(4'-ethylphenoxy)-3,7-dimethyl-6,7-epoxy-trans-2-octene and related compounds. J Agric Food Chem 1974;22(3):386–95.
[2] Hammock BD, Gill SS, Stamoudis V, Gilbert LI. Soluble mammalian epoxide hydratase: action on juvenile hormone and other terpenoid epoxides. Comp Biochem Physiol B 1976;53(2):263–5.
[3] Cronin A, Mowbray S, Dürk H, Homburg S, Fleming I, Fisslthaler B, et al. The N-terminal domain of mammalian soluble epoxide hydrolase is a phosphatase. Proc Natl Acad Sci U S A 2003;100(4):1552–7.
[4] Newman JW, Morisseau C, Harris TR, Hammock BD. The soluble epoxide hydrolase encoded by EPHX2 is a bifunctional enzyme with novel lipid phosphate phosphatase activity. Proc Natl Acad Sci U S A 2003;100:1558–63.
[5] Morisseau C, Hammock BD. Impact of soluble epoxide hydrolase and epoxyeicosanoids on human health. Annu Rev Pharmacol Toxicol 2013;53(1):37–58.
[6] Bellien J, Joannides R, Richard V, Thuillez C. Modulation of cytochrome-derived epoxyeicosatrienoic acids pathway: a promising pharmacological approach to prevent endothelial dysfunction in cardiovascular diseases?. Pharmacol Ther 2011;131(1):1–17.
[7] Fleming I, Simonsen U. The pharmacology of the cytochrome P450 epoxygenase/soluble epoxide hydrolase axis in the vasculature and cardiovascular disease. Pharmacol Rev 2014;66(4):1106–40.
[8] Gomez GA, Morisseau C, Hammock BD, Christianson DW. Structure of human epoxide hydrolase reveals mechanistic inferences on bifunctional catalysis in epoxide and phosphate ester hydrolysis. Biochemistry 2004;43(16):4716–23.
[9] Oguro A, Imaoka S. Lysophosphatidic acids are new substrates for the phosphatase domain of soluble epoxide hydrolase. J Lipid Res 2012;53(3):505–12.
[10] Morisseau C, Schebb NH, Dong H, Ulu A, Aronov PA, Hammock BD. Role of soluble epoxide hydrolase phosphatase activity in the metabolism of lysophosphatidic acids. Biochem Biophys Res Commun 2012;419(4):796–800.
[11] Kramer JS, Woltersdorf S, Duflot T, Hiesinger K, Lillich FF, Knöll F, et al. Discovery of first in vivo active inhibitors of soluble epoxide hydrolase (sEH) phosphatase domain. J Med Chem 2019;62:8443–60.
[12] EnayetAllah AE, Luria A, Luo B, Tsai H-J, Sura P, Hammock BD, et al. Opposite regulation of cholesterol levels by the phosphatase and hydrolase domains of soluble epoxide hydrolase. J Biol Chem 2008;283(52):36592–8.
[13] Oguro A, Sakamoto K, Suzuki S, Imaoka S. Contribution of hydrolase and phosphatase domains in soluble epoxide hydrolase to vascular endothelial growth factor expression and cell growth. Biol Pharm Bull 2009;32(12):1962–7.
[14] Hou HH, Liao YJ, Hsiao SH, Shyue SK, Lee TS. Role of phosphatase activity of soluble epoxide hydrolase in regulating simvastatin-activated endothelial nitric oxide synthase. Sci Rep 2015;5:13524.
[15] Lien C-C, Chen C-H, Lee Y-M, Guo B-C, Cheng L-C, Pan C-C, et al. The phosphatase activity of soluble epoxide hydrolase regulates ATP-binding cassette transporter-A1-dependent cholesterol efflux. J Cell Mol Med 2019;23(10):6611–21.
[16] Sinal CJ, Miyata M, Tohkin M, Nagata K, Bend JR, Gonzalez FJ. Targeted disruption of soluble epoxide hydrolase reveals a role in blood pressure regulation. J Biol Chem 2000;275(51):40504–10.
[17] Luria A, Weldon SM, Kabcenell AK, Ingraham RH, Matera D, Jiang H, et al. Compensatory mechanism for homeostatic blood pressure regulation in Ephx2 gene-disrupted mice. J Biol Chem 2007;282(5):2891–8.
[18] Luria A, Bettaieb A, Xi Y, Shieh G-J, Liu H-C, Inoue H, et al. Soluble epoxide hydrolase deficiency alters pancreatic islet size and improves glucose homeostasis in a model of insulin resistance. Proc Natl Acad Sci U S A 2011;108(22):9038–43.
[19] Keserü B, Barbosa-Sicard E, Schermuly RT, Tanaka H, Hammock BD, Weissmann N, et al. Hypoxia-induced pulmonary hypertension: comparison of soluble epoxide hydrolase deletion vs. inhibition. Cardiovasc Res 2010;85:232–40.
[20] Li L, Li N, Pang W, Zhang Xu, Hammock BD, Ai D, et al. Opposite effects of gene deficiency and pharmacological inhibition of soluble epoxide hydrolase on cardiac fibrosis. PLoS ONE 2014;9(4):e94092.
[21] Cronin A, Homburg S, Dürk H, Richter I, Adamska M, Frère F, et al. Insights into the catalytic mechanism of human sEH phosphatase by site-directed mutagenesis and LC-MS/MS analysis. J Mol Biol 2008;383(3):627–40.
[22] Li D, Qiu Z, Shao Y, Chen Y, Guan Y, Liu M, et al. Heritable gene targeting in the mouse and rat using a CRISPR-Cas system. Nat Biotechnol 2013;31(8):681–3.
[23] Remy S, Chenouard V, Tesson L, Usal C, Ménoret S, Brusselle L, et al. Generation of gene-edited rats by delivery of CRISPR/Cas9 protein and donor DNA into intact zygotes using electroporation. Sci Rep 2017;7:16554.
[24] Morisseau C, Wecksler AT, Deng C, Dong H, Yang J, Lee KSS, et al. Effect of soluble epoxide hydrolase polymorphism on substrate and inhibitor selectivity and dimer formation. J Lipid Res 2014;55(6):1131–8.
[25] Kirkham TC, Williams CM, Fezza F, Di Marzo V. Endocannabinoid levels in rat limbic forebrain and hypothalamus in relation to fasting, feeding and satiation: stimulation of eating by 2-arachidonoyl glycerol. Br J Pharmacol 2002;136:550–7.
[26] McIntyre TM, Pontsler AV, Silva AR, St Hilaire A, Xu Y, Hinshaw JC, et al. Identification of an intracellular receptor for lysophosphatidic acid (LPA): LPA is a transcellular PPARgamma agonist. Proc Natl Acad Sci U S A 2003;100:131–6.
[27] Lasar D, Rosenwald M, Kiehlmann E, Balaz M, Tall B, Opitz L, et al. Peroxisome Proliferator Activated Receptor Gamma Controls Mature Brown Adipocyte Inducibility through Glycerol Kinase. Cell Rep 2018;22(3):760–73.
[28] Lynes MD, Leiria LO, Lundh M, Bartelt A, Shamsi F, Huang TL, et al. The cold-induced lipokine 12,13-diHOME promotes fatty acid transport into brown adipose tissue. Nat Med 2017;23(5):631–7.
[29] Inokuma K, Ogura-Okamatsu Y, Toda C, Kimura K, Yamashita H, Saito M. Uncoupling protein 1 is necessary for norepinephrine-induced glucose utilization in brown adipose tissue. Diabetes 2005;54:1385–91.
[30] Saito M. Brown adipose tissue as a regulator of energy expenditure and body fat in humans. Diabetes Metab J 2013;37:22–9.

[31] Covian R, Balaban RS. Cardiac mitochondrial matrix and respiratory complex protein phosphorylation. Am J Physiol Heart Circ Physiol 2012;303(8):H940–66.
[32] Vanella L, Canestraro M, Lee CR, Cao J, Zeldin DC, Schwartzman ML, et al. Soluble epoxide hydrolase null mice exhibit female and male differences in regulation of vascular homeostasis. Prostaglandins Other Lipid Mediat 2015;120:139–47.
[33] Singh SP, Schragenheim J, Cao J, Falck JR, Abraham NG, Bellner L. PGC-1 alpha regulates HO-1 expression, mitochondrial dynamics and biogenesis: Role of epoxyeicosatrienoic acid. Prostaglandins Other Lipid Mediat 2016;125:8–18.
[34] Shin H, Ma Y, Chanturiya T, Cao Q, Wang Y, Kadegowda AKG, et al. Lipolysis in brown adipocytes is not essential for cold-induced thermogenesis in mice. Cell Metab 2017;26(5):764–777.e5.
[35] Harris TR, Hammock BD. Soluble epoxide hydrolase: gene structure, expression and deletion. Gene 2013;526(2):61–74.
[36] Oelkrug R, Goetze N, Exner C, Lee Y, Ganjam GK, Kutschke M, et al. Brown fat in a protoendothermic mammal fuels eutherian evolution. Nat Commun 2013;4:2140.
[37] Yang Y-M, Sun D, Kandhi S, Froogh G, Zhuge J, Huang W, et al. Estrogen-dependent epigenetic regulation of soluble epoxide hydrolase via DNA methylation. Proc Natl Acad Sci U S A 2018;115(3):613–8.
[38] Mengel LA, Seidl H, Brandl B, Skurk T, Holzapfel C, Stecher L, et al. Gender Differences in the response to short-term cold exposure in young adults. J Clin Endocrinol Metab 2020;105(5):e1938–48.
[39] Gangadhariah MH, Dieckmann BW, Lantier L, Kang Li, Wasserman DH, Chiusa M, et al. Cytochrome P450 epoxygenase-derived epoxyeicosatrienoic acids contribute to insulin sensitivity in mice and in humans. Diabetologia 2017;60(6):1066–75.
[40] Luo P, Chang H-H, Zhou Y, Zhang S, Hwang SH, Morisseau C, et al. Inhibition or deletion of soluble epoxide hydrolase prevents hyperglycemia, promotes insulin secretion, and reduces islet apoptosis. J Pharmacol Exp Ther 2010;334(2):430–8.
[41] Roche C, Besnier M, Cassel R, Harouki N, Coquerel D, Guerrot D, et al. Soluble epoxide hydrolase inhibition improves coronary endothelial function and prevents the development of cardiac alterations in obese insulin-resistant mice. Am J Physiol Heart Circ Physiol 2015;308(9):H1020–9.
[42] Heusch G, Schulz R, Rahimtoola SH. Myocardial hibernation: a delicate balance. Am J Physiol Heart Circ Physiol 2005;288(3):H984–99.
[43] Purba ER, Leuhery EA, Oguro A, Imaoka S. The metabolism of lysophosphatidic acids by allelic variants of human soluble epoxide hydrolase. Drug Metab Pharmacokinet 2015;30(1):75–81.
[44] Ramirez CE, Shuey MM, Milne GL, Gilbert K, Hui N, Yu C, et al. Arg287Gln variant of EPHX2 and epoxyeicosatrienoic acids are associated with insulin sensitivity in humans. Prostaglandins Other Lipid Mediat 2014;113–115:38–44.
[45] Ma L, Yan M, Kong X, Jiang Y, Zhao T, Zhao H, et al. Association of EPHX2 R287Q polymorphism with diabetic nephropathy in chinese type 2 diabetic patients. J Diabetes Res 2018;2018:1–6.
[46] Fava C, Montagnana M, Danese E, Almgren P, Hedblad B, Engström G, et al. Homozygosity for the EPHX2 K55R polymorphism increases the long-term risk of ischemic stroke in men: a study in Swedes. Pharmacogenet Genomics 2010;20:94–103.
[47] Oni-Orisan A, Cresci S, Jones PG, Theken KN, Spertus JA, Lee CR. Association between the EPHX2 p.Lys55Arg polymorphism and prognosis following an acute coronary syndrome. Prostaglandins Other Lipid Mediat 2018;138:15–22.